Particle and X-ray damage in pn-CCDs

Norbert Meidinger*, Bernhard Schmalhofer, Lothar Strüder

Max-Planck-Institut für extraterrestrische Physik, Giessenbachstraße, D-85740 Garching, Germany

Abstract

The fully depleted pn-junction charge coupled device (pn-CCD) has been developed as a detector for X-ray imaging and high-resolution spectroscopy for the X-ray satellite missions XMM and ABRIXAS. If the detector is exposed to a particle radiation environment, the energy resolution is degraded due to charge transfer losses and a dark current increase. In a first experiment, prototype devices were irradiated with 10 MeV protons. After completion of the detector development, the proton irradiation was repeated for a quantitative study of the radiation damage, relevant for the satellite missions. The irradiation test was extended by a 5.5 MeV α-particle and a 6 keV X-ray exposure of the pn-CCD, including the CAMEX preamplifier chip.

1. Introduction

1.1. Detector concept

The pn-CCD is a novel charge coupled device type developed for X-ray imaging and spectroscopy in the bandwidth between 0.2 and 15 keV. A highly doped large area boron implant on the backside of the device is used as an ultra-thin homogeneous photon entrance window for low-energy photons (Fig. 1). This results in a quantum efficiency of about 90% at a low photon energy of 500 eV. The fully depleted device thickness of 300 μm increases the quantum efficiency for the high X-ray energies to above 90% at 10 keV. The charge transfer on the device frontside is performed in the 12 μm thick epitaxial layer, with a resistivity of 40 Ω cm, which has been deposited on top of the 5 kΩ cm float-zone high-purity n-type silicon. The 6 cm × 6 cm large flight-type pn-CCD consists of twelve 3 cm × 1 cm large units fabricated monolithically on a single 4 inch silicon wafer. For test purposes, single 3 cm × 1 cm large pn-CCD units with identical design were manufactured with the same fabrication process as the full size detectors. Each pn-CCD unit consists of 64 charge transfer channels which are 200 pixels deep. The pixel size is 150 μm × 150 μm. Each channel is equipped with an anode which is the gate of an amplifying n-channel junction field effect transistor (JFET) and the source of a second JFET for charge reset. Each source of the first amplifying FET is connected by a bond wire with one of the 64 inputs of the preamplifying and multiplexing CAMEX64B chip. The CAMEX clocking is controlled by a digital chip called TIMEX. The fabrication and performance of the flight-type pn-CCDs are described in Refs. [1,2] of this issue.

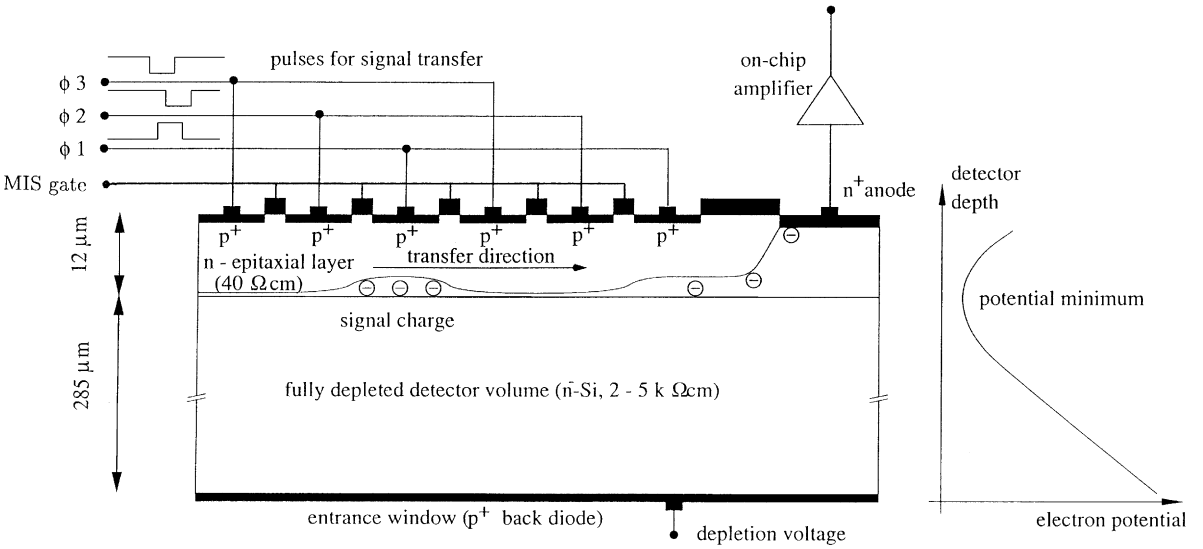

Fig. 1. A schematic cross section through the fully depleted pn-CCD along a transfer channel. The photon entrance window and the charge transfer registers, $\varphi 1$, $\varphi 2$, $\varphi 3$, on opposite wafer surfaces are realized through p^+-implantations in n-type silicon. The surface potential between the registers is determined by metal–nitride–oxide–silicon gates. The entering X-ray photons generate electrons in the silicon which are collected and transferred in a depth of 11 µm below the registers in the epitaxial layer. When the signal charge packet has reached the anode, it is amplified on the CCD-chip by a JFET whose source is connected with a preamplifier channel in a source follower configuration.

1.2. Application: XMM and ABRIXAS

The 36 cm^2 large pn-CCD will be used for two X-ray astronomy satellite missions. The first one is the X-ray Multi Mirror (XMM) mission of the European Space Agency [3]. The satellite will be launched in January 2000 and perform pointed observations of the X-ray sky in the bandwidth of 0.2–15 keV. One of its three telescopes will be equipped with a pn-CCD camera as focal plane instrumentation. The X-ray photons will be focussed by a Wolter telescope with a focal length of 7.5 m. The denotation "Multi" of XMM refers to the number of 58 mirror modules per telescope.

The second satellite performs an all sky survey complementary to the XMM pointing observations. This German mission is called according to its objective target, A BRoad-band Imaging X-ray All-sky Survey (ABRIXAS) [4]. Since the mission starts already in spring of 1999, it will work as a pathfinder for the XMM mission. Seven Wolter telescopes with a focal length of 1.6 m will focus the X-ray photons on seven different areas of the 6 cm × 6 cm large pn-CCD detector.

Radiation damage to the pn-CCD sensors is caused by solar flares, when crossing of the radiation belts (especially for XMM with the highly eccentric orbit), and by cosmic rays. The damage will accumulate during the mission time which, in the case of XMM, lasts 10 years and for ABRIXAS three years. CCDs in general are fairly sensitive to radiation damage since silicon lattice defects, caused by irradiation, affect the charge transfer by trapping. The slow transfer of a small number of signal electrons (between 50 and 4000 electrons depending on the X-ray photon energy) over distances in the order of 10 mm can then result in significant signal losses. Therefore radiation damage must be held at a minimum to maintain the high spectral resolution of the detector until the end of the mission. This will be achieved by a thick shielding of the detector and by the design of the pn-CCD. Furthermore the effects of radiation damage can be softened by the appropriate choice of

operating conditions. Finally, the charge transfer losses have to be studied to correct them as well as possible.

1.3. Radiation damage relevant changes from prototype to flight-type pn-CCD

The first radiation damage tests, dating back to 1995 [5], were performed with 1 cm × 1 cm large prototype pn-CCDs. They had transfer channels which were 60 pixels deep compared to the 200 pixels of the present devices.

For the flight-type devices the transfer channels in the 150 μm × 150 μm pixels were narrowed to reduce the charge transfer losses by trapping. This was accomplished by a phosphorus implantation in the middle of the transfer channel and enforced by a deep boron implantation between the channels.

The new design offers the possibility of charge injection into the last pixel per channel by an electrode. The traps in all pixels can then be occupied due to the charge transfer of the injected electrons during the readout of the image. As a result the charge transfer losses of the X-ray signals of the next image are decreased if the occupation lasts that long.

The prototype devices were manufactured with 3 inch silicon wafers whereas, for the flight-type CCDs and the new small size test CCDs, 4 inch material was taken to realize the 36 cm^2 large monolithic CCD. In spite of a similar resistivity and fabrication process, the impurity concentrations of the new silicon might be different. This in turn, can change the radiation hardness due to different lattice defect generation rates.

1.4. Summary of previous results

The measurements after the proton irradiations of the small prototypes had shown that the pn-CCDs are radiation harder than conventional X-ray CCDs. The results and the reasons for the radiation hard pn-CCD concept were presented in Refs. [5,6]. The charge transfer efficiency (CTE) is the device characteristics which is most susceptible to particle exposure. The reason for this sensitivity is the generation of oxygen-vacancy defects (A-centres) in the silicon lattice which trap signal electrons during their transfer to the anode. If the trapped electrons are released too late to be transferred with the other signal charges, this results in charge transfer loss. It is expressed in terms of charge transfer inefficiency (CTI), with the charge transfer efficiency (CTE) as its complement. CTI = 1 − CTE means thereby the fraction of non-transferred electrons per pixel compared to the number of electrons before the transfer. The radiation damage affects the CTE most strongly at an operating temperature of about 120 K. An efficient thermal annealing of the A-centre is obtained with a temperature of 350°C which is too high to be applied to the detector in the satellite. The charge transfer losses could be minimized by increasing the transfer speed which reduces the trapping probability. The effects of trapping on the charge transfer and their dependence on operating parameters and photon environment were studied and described by a model [6].

The 10 MeV proton irradiation was repeated for the flight-type devices. The radiation damage experiments were completed by 5.5 MeV α-particle and 6 keV X-ray photon exposures. A description of the experiment and first results were presented in Ref. [7]. Two trap types could be observed which were already present before irradiation and two traps types were generated by particle irradiation. The concentration of the most significant particle generated trap type, the A-centre, rises linearly with the particle fluence. Its generation probability does not depend on the temperature during irradiation and is nearly the same for the individual samples of the flight-type devices. The nonionizing energy loss (NIEL) in orbit which causes the defect generation in the CCD, will be mainly due to protons. The NIEL is equivalent for XMM to that by 10 MeV protons with a fluence of roughly 5×10^8 cm^{-2}. For ABRIXAS it will be less because of the lower orbit and the shorter mission time. The energy resolution of the Mn-K_α line (5894 eV) is only weakly degraded after the total proton fluence expected for both satellite missions. The second of the two trap types which were generated by the particle exposure, is presumably the divacancy (vacancy–vacancy defect). It effectuates less charge transfer losses than the A-centre. The ratio of divacancies to A-centres is higher after a 5.5 MeV α-particle

irradiation than after a 10 MeV proton exposure. This is caused by the higher ratio of "nonionizing energy loss" to "ionizing energy loss" of the 5.5 MeV α-particle compared with that of the 10 MeV proton.

1.5. Objectives of this study

The previous analysis concentrated on the charge transfer loss. We now compare the radiation damage of the prototype to the flight-type pn-CCDs. The charge transfer loss of the new devices has been improved by a narrowing of the transfer channel and by the possibility of periodical charge injection during operation.

The defects generated by particle irradiation, can behave not only as traps but also as generation centres for electron–hole pairs, i.e. cause an increase of the dark current. Therefore, we measured the dark current as function of the temperature before and after irradiation.

During the proton exposures, the CAMEX pre-amplifier and the TIMEX chip were shielded in the manner as the detector had to be mounted in the experiment. However, during the α-particle and X-ray bombardment, both components were irradiated.

As a first result on the pn-CCD performance degradation, the energy resolution of the Mn-K_α line was presented as function of the proton fluence [7]. The analysis will now be completed by studying other X-ray energies, especially low-energy X-rays.

Finally, the energy resolution is studied as function of the charge transfer loss.

2. Radiation damage

Radiation damage means here a disadvantageous change of device parameters which is caused by radiation exposure. This may result in a change of operating parameters or a nonrecoverable degradation of the device key characteristics.

2.1. Output characteristics of the on-chip electronics

The pn-CCD on-chip electronics consist of two JFETs per transfer channel. One is used for a first signal charge amplification, the other for clearing the anode charge. The radiation hardness of the JFET output characteristics was studied with an early detector version exposed to a relative severe 10 MeV proton environment compared to the satellite missions. It turns out that the transistor output characteristics is only slightly changed after a fluence of 2.6×10^{11} cm^{-2} (see Fig. 2). The uniform shift is probably due to a change in the standard ambient conditions between the measurements. The effect of radiation exposure on the JFET noise is studied in Section 3.2.

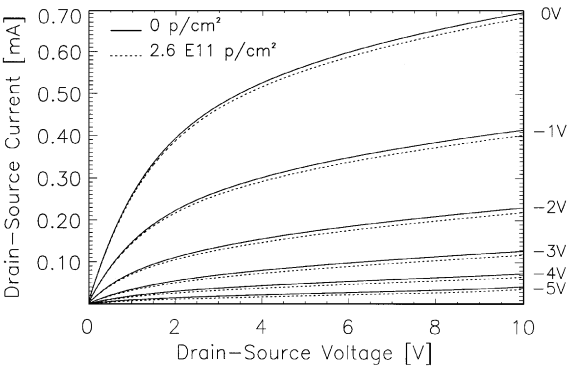

Fig. 2. Output characteristics of the n-channel junction field effect transistor. The on-chip electronics of the pn-CCD consist of one JFET for amplification and one for the reset of the charge on the anode. The solid lines show the characteristics as a function of different gate voltages ($0, -1, \ldots, -5$ V) before radiation exposure. The dotted curves were measured a few days after a 10 MeV proton exposure of 2.6×10^{11} p/cm^2. The slight shift of the curves is probably due to a small change in the ambient conditions under which the measurements were performed.

2.2. Flatband voltage

Metal–insulator–silicon (MIS) gates are implemented between the 10 mm long transfer registers of the pn-CCD. They consist of a 3000 Å thick SiO_2-layer and a 1450 Å thick Si_3N_4-layer covered by 1 μm of aluminium. The gates are kept at a constant potential and determine the electrical potential of the surface between the clocked pn-diode registers. While pn-structures are only slightly deteriorated, MIS-structures are more susceptible to radiation exposure. Particle irradiation creates new interface traps between insulation layer and silicon. In addition, a positive charge build up

Table 1
Flatband voltage of the MIS-gates which are implemented between the transfer registers on the pn-CCD. The insulating layer consists of 3000 Å SiO_2 and 1450 Å Si_3N_4 and is covered by 1 μm of aluminium. The flatband voltage of three different test devices was measured before, one week after and 6 months after a 10 MeV proton exposure. The nonlinear shift of the flatband voltage with increasing proton fluence is not yet understood. Possibly, the flatband voltage shift is strongly determined by the proton flux which was increasing for the three samples

Device Proton fluence	#1 5E8 p/cm^2	#2 2E9 p/cm^2	#3 5E9 p/cm^2
Before irradiation	− 5.61 V	− 4.9 V	− 4.9 V
1 week after irradiation	− 5.76 V	− 12.0 V	− 13.5 V
6 months after irradiation	− 5.70 V	− 10.7 V	− 11.8 V

occurs in the insulating layer by ionizing radiation. The radiation damage in the MIS gates was characterized by the measurement of the flatband voltage. A frequency of 20 Hz was chosen to measure capacitance in order to also take into account the slow charge movement and low-frequency interface states. The flatband voltages of three test devices were measured before irradiation, a few days after the proton exposure and 6 months after the exposure. The results are given in Table 1. Before irradiation, the flatband voltage has a value of about − 5 V for all devices. After the proton exposure, the flatband voltages increase with the fluence up to − 13.5 V at 5×10^9 cm^{-2}. However, the rise was not linear for the three devices. The decrease within 6 months of storage at room temperature was about 40% for the lowest proton fluence and about 20% for the two higher fluences. The nonlinear shift of the flatband voltage of the devices with the proton fluence is possibly caused by their susceptibility to the particle flux which rose with the fluence. As a consequence, a smaller flatband voltage shift is expected for the mission than measured in the tests because the fluxes used in the irradiation experiment simulate within several hours a radiation fluence which will accumulate in the whole mission time.

2.3. Dark current

2.3.1. Dark current increase with bias voltage at room temperature

The phosphorus-doped bulk becomes depleted if a negative voltage is applied to the large area p^+-contact of the pn-CCD backside. With a voltage of approximately − 100 V, the 285 μm thick layer of the high-resistivity silicon (5 kΩ cm) is depleted. The dark current of the bulk contact was measured as function of the bias voltage before and after the proton exposure (Fig. 3). The measurement of the diode characteristics was repeated every few days after proton irradiation to study self-annealing effects. The measurements were carried out in a dark box at a temperature of 22°C ± 2°C, all under ambient conditions. Before irradiation, the dark current per cm^2 varied for the tested pn-CCDs between 2 and 8 nA at a bias voltage of − 100 V.

The current increase after radiation exposure can be characterized by the k-factor [ampere/proton] which is defined as the dark current increase per proton:

$$\Delta I = k \cdot \# \text{ protons} \quad (1)$$

where ΔI is the total current increase after # protons.

One day after irradiation the k-value was in the range of $1.2\text{–}2.5 \times 10^{-16}$ A/p. Forty days after the proton irradiation, the damage factor had dropped to almost half of the initial value for each device: $k = 0.7\text{–}1.5 \times 10^{-16}$ A/p. For an acceleration of recovery, one device was heated up to a temperature of 50°C for 20 h and later to 70°C for 20 h. However, no significant decrease of the dark current could be observed after these annealing steps.

The measured dark current consists of two components: The surface current which remains close

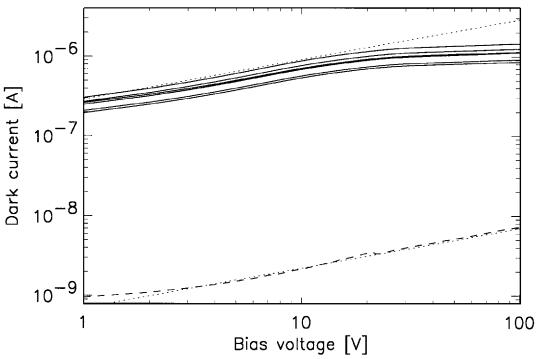

Fig. 3. Dark current of a 3 cm^2 large pn-CCD measured at ambient conditions as a function of the bias voltage which was applied between the p^+-implantation of the entrance window and the n-bulk. The dashed line shows the dark current before irradiation. It increases with the depletion volume as expected for a bulk generation current. The theoretical rise according to Eq. (2) is depicted by the dotted line. The solid lines show the current after a 10 MeV proton exposure of 5.8×10^9 cm^{-2}. A steep increase to 3×10^{-7} A occurred below a voltage of 1 V. The measurement was repeated every few days up to forty days to study the slow but continuous recovery of the dark current due to self-annealing. The current increase with the bias voltage above a voltage of 20 V is smaller than expected for a bulk current. The upper dotted line depicts for comparison the bulk generation current according to Eq. (2) under the assumption of an 3×10^{-7} A current offset. The dark current after irradiation is obviously not determined by the bulk current but mainly by the surface current.

to the surface and the bulk current which is collected in the pixels and transferred to the anodes. The number of thermally generated electrons (and holes) in the bulk is proportional to the bias volume, if we assume a homogeneous distribution of generation centres. This is in a first approximation valid for 10-MeV protons since their nonionizing energy loss per unit length varies only by about one third in the depth of the silicon device. The volume is given by the area of the entrance window and the depletion depth. The depth is proportional to the square root of the bias voltage V and inverse proportional to the doping concentration N_d which is constant within the high-resistivity bulk. The drift current I_{drift} is hence determined by

$$I_{drift} \sim \sqrt{V/N_d}$$
$$\log(I_{drift}) = \text{const} + \tfrac{1}{2}\log V. \tag{2}$$

(For bias voltages V not too small ($V \gg V_{built\text{-}in}$), the diffusion current contribution can be neglected.) Before irradiation, the dark current rises with the bias voltage according to Eq. (2), as we expect for bulk generation current. However, this is no longer valid after proton irradiation (see Fig. 3). After irradiation, we have to consider the effect of a higher nonionizing energy loss and therefore a higher defect concentration with decreasing proton energy. Since the protons entered the device from the backside and the depletion starts from the same device side, the higher bulk current increase would be expected for the high bias voltages. However, instead of a slightly higher current rise as function of the bias voltage, a substantial smaller current rise is observed. This shows that the radiation-induced increase of dark current is not dominated by bulk damage but by surface damage. This is important since the bulk current is collected in the pixels while the surface-generated current is drained without contributing to the signal.

2.3.2. Bulk dark current increase with temperature

One contribution to the noise of the detector is determined by the number of dark current electrons which are collected during the cycle time in a pixel. Its volume is limited by the area of 150 μm × 150 μm and the fully depleted chip thickness of 300 μm. The contribution increases with rising temperature because of the thermal generation of electron–hole pairs. The thermal generation current j_{gen} in the pn-CCD shows the following temperature dependence according to the theory of Shockley–Read–Hall with a few assumptions for simplification, e.g. that the generation centres are located in the middle of the band gap E_g:

$$j_{gen} \sim T^2 \exp\left(\frac{-E_g}{2kT}\right) \tag{3}$$

with k as the Boltzmann constant and T as the absolute temperature.

On account of particle irradiation, new generation centres are produced in the silicon lattice. Hence the thermally generated dark current in the bulk increases, i.e. at the same temperature, a higher number of electrons is collected in the pixels than

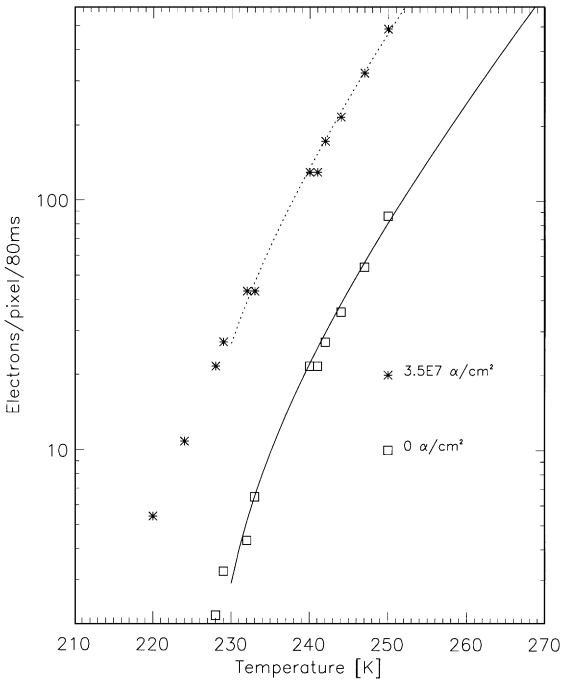

Fig. 4. Number of dark current electrons which were collected in a pixel within the cycle time of 80 ms as a function of the temperature. The squares depict the current before irradiation and the asterisks after a 5.5 MeV alpha particle exposure of 3.5×10^7 per cm^2. The current into the pixels is increased by almost one order of magnitude after the irradiation. The curves above 230 K were obtained by a fit to the experimental data according to Eq. (3). For the fit, a temperature-independent constant is added to consider an electron generation due to a residual level of infrared and visual light (see Section 2.4.1).

before irradiation. Fig. 4 shows the measured average number of dark current electrons collected in the pixels per cycle time as function of the temperature before and after irradiation. The cycle time means the photon accumulation time including the readout time for one image. It took 80 ms in our tests which is close to the cycle time of 73 ms for the 6 cm × 6 cm large flight detectors in orbit. Without particle irradiation, the dark current per pixel and image increases steeply from two electrons at 228 K up to 90 electrons at 240 K. These values vary of course for individual samples of pn-CCDs of same type. After a 5.5 MeV alpha particle fluence of 3.5×10^7 per cm^2, the current level is 10 times higher than before the irradiation.

2.4. Charge transfer inefficiency

In this section we describe the charge transfer losses of the flight-type pn-CCDs. They are compared with that of the prototype devices, and the method of charge injection is tested. Finally we evaluate an upper limit for the not trap dependent charge transfer losses.

2.4.1. CTI of prototype and flight-type devices

The charge transfer loss differs slightly between individual pn-CCDs of the same design and fabrication process. Significant changes of CTI are mostly caused by different operating voltages or a different clocking scheme of the detector (e.g. see Figs. 11 and 12 in Ref. [6]). Before irradiation, the flight-type pn-CCDs show charge transfer losses at 180 K by about a factor of five less than the prototype devices of same size (Fig. 5). The better CTE is mainly due to the narrowed transfer channel. For the prototype pn-CCDs, the CTE was found to be dependent on the number of pixels in the transfer channel. The maximum charge transfer loss per pixel along the 10 mm long and 60 pixel deep channels were only half of that of the 30 mm and 200 pixel deep devices. The explanation for this observation is given by the infrared light emission [8] of the CAMEX preamplifier which is mounted nearby the on-chip electronics of the pn-CCD. This infrared light close to 1100 nm wavelength, generates with a low quantum efficiency electron–hole pairs, showing up like leakage current. Since the intensity of the infrared light decreases with increasing distance of the pixels to the CAMEX, the continuous generation of single electrons decreases as well. Therefore, the concentration of empty traps and thus the trapping probability increases with the distance to the CAMEX. As a result, the CTE is generally better for pn-CCDs with shorter transfer channels. This effect is not as temperature dependent as the method of periodical charge injection once per image. (see Fig. 7 and Section 2.4.3).

The CTE is only degraded after irradiation with particles but not after a 23 krad dose of soft X-rays. This was expected since the X-ray photons need an energy of at least 200 keV to cause a displacement damage in the silicon lattice which is a prerequisite

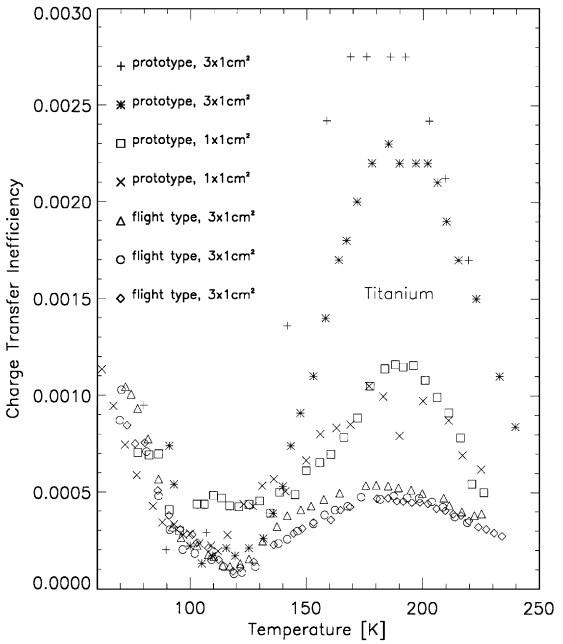

Fig. 5. Charge transfer inefficiency of flight-type and prototype pn-CCDs without radiation damage. The flight-type devices show the lowest charge transfer loss because of the transfer channel narrowing. The maximum CTI is by a factor of five lower than that of the prototype devices with the same size. These 30 mm long and 200 pixel deep prototypes show a maximum CTI which again is by a factor of two higher than that of the 10 mm long and 60 pixel deep prototypes. The difference due to the transfer channel length is caused by the infrared light emission of the preamplifier which reduces the empty trap concentration for the pixels close to the CAMEX chip. The CTI peak at 180 K is due to the titanium trap, whereas the deterioration of the charge transfer at temperatures below 100 K is caused by another unidentified trap type.

for trap generation. After proton and α-particle irradiation, the charge transfer losses were increased in the whole temperature regime from 70 to 230 K (see Fig. 6). They are about a factor of 1.5 higher at the CTI maximum for the flight-type pn-CCDs than for the 10 mm prototype devices. This is in contrast to the results before particle exposure, where the flight-type pn-CCDs had transfer losses lower by a factor of 2. If we assume the same trap concentration for the prototype and the flight-type devices before irradiation and take into account the linear increase of CTI with the trap concentration (see Fig. 5 in Ref. [7]), we get an A-centre (oxygen-vacancy defect) generation probability which is higher by a factor of 3 for the flight-type devices. Since there is no reduction in the concentration of phosphorus which competes with the oxygen for the vacancy, we conclude that the new 4 inch silicon wafer charge has by a factor of 3 higher oxygen concentration than the 3 inch silicon charge used for the prototypes.

2.4.2. CTI dependence on operating temperature and traps

The study of trapping effects on the charge transfer in pn-CCDs [6] explains why a CTI versus temperature curve shows a peak for each trap type. The characteristic trap parameters, i.e. the energy level $E_c - E_t$ of the defect referred to the conduction band edge of silicon and the capture cross section σ_c, determine together with the temperature the emission time constant of the trap type:

$$\tau_e \sim \frac{1}{\sigma_c} \exp\left(\frac{E_c - E_t}{kT}\right). \tag{4}$$

If the emission time is much longer than the cycle time, i.e. below a temperature characteristic for the trap type, most of the traps remain occupied when the next signal charges are transferred. As a result the CTI is low. If the emission time constant is shorter than the time for one pixel transfer, i.e. above a characteristic temperature, most trapped electrons are released fast enough to still be kept in the same charge packet. But for the temperature in between, neither most of the traps are occupied, nor the release of electrons is in good time to keep the charge loss small. We obtain the maximum CTI at this characteristic temperature which is different for each trap type due to different energy levels and capture cross sections (see Figs. 5 and 6). Above a temperature of 200 K the height and shape of a CTI peak is affected by the increased dark current which saturates traps. Finally, at temperatures far above 200 K, no CTI can be measured. The noise contribution by the dark current is then too high for an exact determination of the charge transfer losses.

Temperature scans were carried out with the flight-type devices for a trap evaluation as well as for an analysis of the detector performance to find

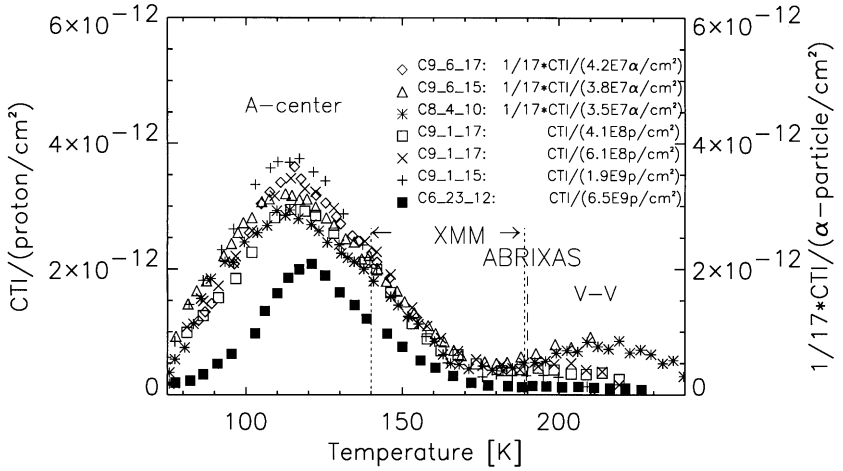

Fig. 6. Charge transfer inefficiency per particle fluence of flight-type and prototype pn-CCDs after proton and α-particle exposure. The main CTI peak at a temperature of 115 K is caused by trapping the signal electrons in the generated A-centres. The smaller peak at higher temperatures occurring after α-particle irradiation is assumed to be due to divacancies. A 5.5 MeV α-particle causes 17 times higher charge transfer losses by the A-centres than a 10 MeV proton. The difference in the divacancy generation probability is considerably higher. The proton irradiated prototype device (C6_23_12 with 60 pixel deep transfer channel, depicted by black squares in the figure) had suffered smaller charge transfer losses in spite of its broad transfer channel compared with the flight-type CCDs. Thus we conclude that the A-centre generation probability was higher for the flight-type CCDs than for the prototype devices, as a result of a higher oxygen concentration in the silicon.

the best operating temperature. The temperature scans in Figs. 5 and 7 show that without particle exposure one dominant trap type, a titanium impurity [9], limits the charge transfer above 110 K. It causes a charge transfer loss maximum at a temperature of 180 K. Below 110 K, another trap-type degrades the charge transfer up to a factor of two more than the titanium trap. The maximum charge transfer loss occurs below a temperature of 70 K. Due to this fact, that trap-type does not affect the detector performance in the pn-CCD operating temperature range of 140–190 K to be used for the satellite missions.

The CTI increase per particle and cm^2 as function of the temperature is depicted in Fig. 6. The temperature scans after the proton and α-particle irradiations show that the A-centre is the dominant trap type for all devices. It causes the maximum degradation at a temperature of about 115 K. For all flight-type devices, approximately the same CTI increase per proton and per α-particle respectively, was obtained. Hence, the A-centre generation rate is rather similar for the devices which were produced with silicon of the same batch. Fig. 6 shows that the A-centre generation probability is about a factor of 17 higher for a 5.5 MeV α-particle damage than for a 10 MeV proton damage.

The temperature scan in Fig. 6 shows a second particle generated trap type with maximum charge transfer losses at a temperature of about 210 K. There are indications that this trap is a divacancy defect. Firstly, Monte Carlo simulations and Deep Level Transient Spectroscopy measurements (just as in Ref. [6]) suggest this trap type. Secondly, a 5.5 MeV α-particle generates along its short range of 27 μm a much higher vacancy concentration and thus an enhanced divacancy formation probability than a 10 MeV proton with a smaller energy deposition of 2.9 MeV along its path through the 300 μm thick device. The divacancies were therefore more so generated by the α-particle exposure (see Fig. 6).

2.4.3. CTI improvement by charge injection

In contrast to the prototype devices, the flight-type CCDs provide the possibility of electron injection into the last pixel of each transfer channel. By

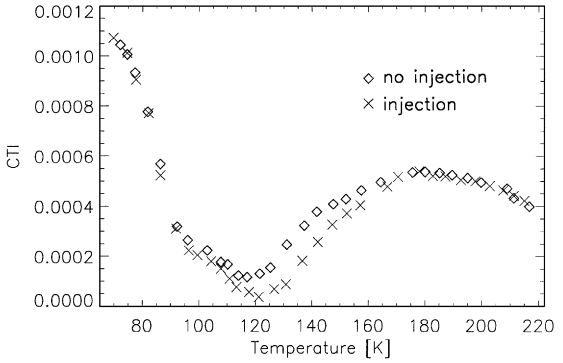

Fig. 7. The figure shows the effect of charge injection on the CTI before particle exposure. The charge injection in the order of 1000 electrons per channel and cycle time of 80 ms, improves the CTI considerably at a temperature of 120 K. The difference in the titanium trap occupation, with and without the use of charge injection once per image, is then maximal. The effect of charge injection is less effective at higher temperatures since most of the injected electrons are released from the traps before the signal charges are transferred. For the same reason, no change in CTI can be observed between 70 and 100 K where the second trap type dominates.

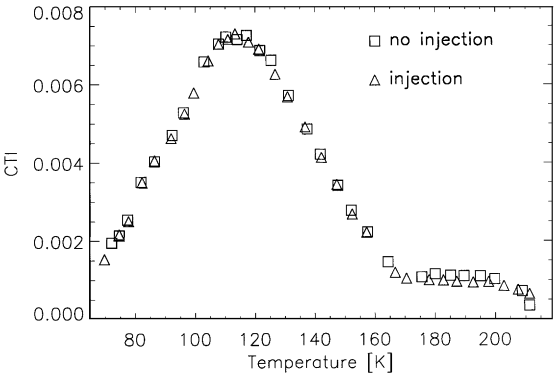

Fig. 8. The figure shows the effect of the charge injection on the CTI after a 10 MeV proton exposure of 1.9×10^9 cm^{-2}. The charge injection does not improve the CTI significantly which is already degraded by A-centre traps. The best improvement is obtained at a temperature of 190 K due to the occupation of the divacancy traps.

the transfer of the injected charge over all 200 pixels to the anodes during the readout of the image, the traps are partially occupied. This decrease of the empty trap concentration holds for a time determined by the emission time of the traps or longer since the injected electrons are captured again during the transfer [6]. As a consequence, the CTI improvement can be effective as long as the emission time constant of the trap type is longer than the injection period (80 ms). The emission time decreases with increasing temperature according to Eq. (4). Without particle exposure, a charge injection in the order of 1000 electrons per channel and cycle time shows a significant CTI improvement between 110 K and 160 K (Fig. 7). The injected electrons occupy the titanium trap most effectively at a temperature of 120 K. The charge transfer losses are decreased by almost a factor of four.

After a proton exposure, the CTI is strongly increased and the improvement is relatively small. Fig. 8 depicts the effect of charge injection after a 10 MeV proton fluence of 1.9×10^9 p/cm^2. It gave the best results at a temperature of 190 K due to the occupation of the divacancy traps. A better CTI could be obtained with a larger quantity of injected electrons but the relative improvement was still small.

2.4.4. CTI dependence on operating voltages

The charge transfer potential at a depth of 12 μm is weakly determined by the MIS-gate potential (on top of the oxide in the regions between the p^+ transfer registers). Especially after particle exposure, the best charge transfer performance was measured with a MIS-gate operating voltage of -15 V instead of 0 V. This MIS-voltage was found to be optimal for all proton and α-particle fluences which are presented in Fig. 6. The flatband voltage shift is more then compensated by this MIS gate voltage change according to the measurements presented in Section 2.2. Since the CTI was not affected by the 23 krad X-ray irradiation, we conclude that also the flatband voltage shift is insignificant at this dose level.

2.4.5. Charge transfer loss as function of photon energy

The occupation probability of a trap increases with the number of electrons in the transferred

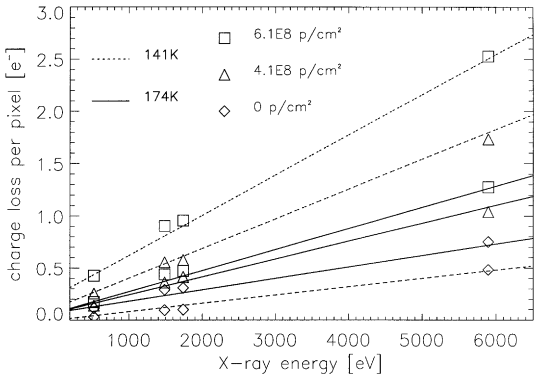

Fig. 9. Charge transfer loss per pixel as function of the photon energy for different proton irradiation fluences and temperatures. The signal electron loss increases with the X-ray energy because of the higher electron capture probability of the traps. For the higher temperature of 174 K (solid lines) the loss is less dependent on proton exposure than for the lower temperature of 141 K (dotted lines).

charge packet [6]. Therefore the loss of signal electrons rises with the X-ray energy. Fig. 9 depicts the measured charge loss per pixel as function of the X-ray energy. We observed for all X-ray energies before proton exposure that the higher temperature of 174 K causes the higher transfer losses than the lower temperature of 141 K. The reason for this is that the CTI of the nonirradiated device is at the high temperature more limited by the titanium trap. The inverse performance is found after proton exposure, a smaller charge transfer loss is obtained with the higher temperature. The generated A-centres affect the charge transfer less at the high temperature because most of the trapped electrons are released after the capture early enough to be transferred with the other signal charges. The figure shows as a result that the charge transfer losses are less irradiation dependent at the higher temperature of 174 K.

2.4.6. CTE dependence on X-ray flux

The CTE dependence on the Mn-K X-ray flux is shown before and after proton irradiation in Fig. 10. The measurements were carried out at different device operating temperatures of 143, 176 and 181 K which cover the typical detector operating temperature range of the satellite missions.

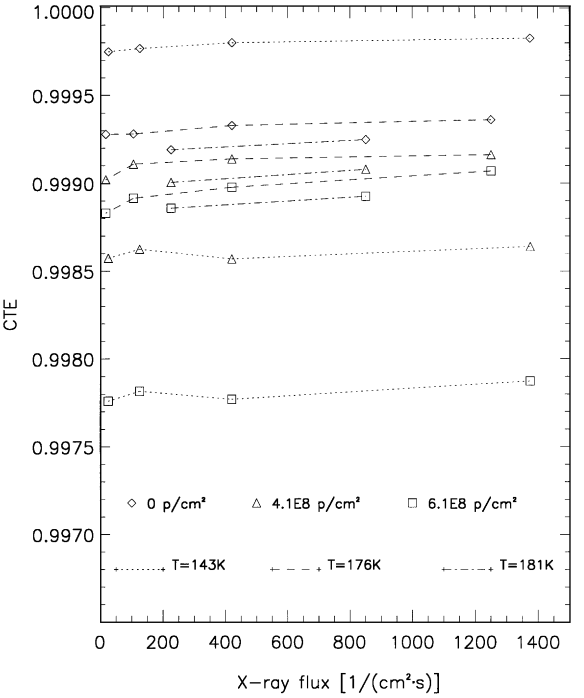

Fig. 10. The charge transfer efficiency of Al-K X-rays (1486 eV) is depicted as a function of their flux for three different temperatures (dotted lines correspond to 143 K, dashed lines to 176 K and dash dot lines to 181 K). The measurements were carried out before irradiation and after two different 10 MeV proton fluences of 4.1×10^8 and 6.1×10^8 cm^{-2}. The CTE rises only slightly with the X-ray flux in the shown temperature range between 143 and 181 K. Only for the lowest temperature of 143 K and before irradiation is the charge loss decreased by about 30%. For the two higher temperatures and after particle irradiation, respectively, the emission times of the titanium trap and A-centre, respectively, are already too short for an effective trap occupation. Thus most of the traps are empty when the next signal charge packet is transferred and the CTE value remains nearly constant.

The CTE is only slightly improved with rising X-ray flux compared to the effect of a temperature change. The maximum charge loss decrease with X-ray flux of about 30% was obtained for the nonirradiated devices at the low operating temperature of 143 K. The emission time of the titanium trap is then sufficiently long that a considerable amount of traps is still occupied when the next signal charge packet is transferred in the same channel. The photon flux is thus for the correction

of the charge transfer loss a parameter of minor importance if we choose an operating temperature above 170 K. A stronger increase of the CTE due to the occupation of the A-centre traps, occurs for higher photon fluxes and a lower operating temperature, i.e. a longer emission time constant. This was already depicted in Fig. 10 of Ref. [6].

2.4.7. Trap-dependent charge transfer losses

The temperature dependence of the charge transfer losses and the effect of charge injection verify that the CTI is determined by trapping and not, for example, by an unfavourable shape of the electric potential during the transfer of the signal charges. Hence, an upper limit for charge transfer losses which are not caused by traps, is seen in Fig. 7 by the minimum CTI of 3.7×10^{-5} at a temperature of 120 K. Figs. 7 and 8 point out that such transfer losses are negligible compared to losses caused by traps, especially after accumulation of radiation damage.

3. Energy resolution

The effects of radiation damage result in a degradation of the energy resolution of the detector. The measured full-width at half-maximum (FWHM) of a spectral line can be expressed by the total noise charge N_{tot}:

$$\mathrm{FWHM[eV]} = 2.355 \times 3.70 \left[\frac{\mathrm{eV}}{\mathrm{e}^-}\right] N_{\mathrm{tot}}[\mathrm{e}^-]. \quad (5)$$

The temperature-dependent electron–hole pair creation energy has a value of 3.70 eV in the relevant temperature range.

The relevant noise contributions are given in the following equation which comprises the Fano noise, the irradiation-dependent transfer noise, the dark current noise and some excess noise:

$$\mathrm{FWHM[eV]} = 2.355 \times 3.70 \sqrt{\frac{FE}{3.70} + N_{\mathrm{trans}}^2 + N_{\mathrm{dark}}^2 + \sum_i N_i^2} \quad (6)$$

where E is the X-ray photon energy [eV], F the Fano factor (0.115), N_{trans} the noise charge [e^-] of charge transfer losses, N_{dark} the noise charge [e^-] of dark current in pixels, and N_i the noise charge [e^-] of the other contributions.

3.1. Noise increase by dark current in the pixels

The dark current electrons which are collected in the pixels during the cycle time, contribute to the total noise. The noise charge N_{dark} of S electrons is determined by the Poisson statistics

$$N_{\mathrm{dark}} = \sqrt{S}. \quad (7)$$

For an evaluation of the noise contribution N_{dark} due to dark current electrons in the pixels, the noise of the normal CCD operation mode N_{normal} and of the backshift operation mode $N_{\mathrm{backshift}}$ are compared. For the backshift mode the charge transfer direction is reversed. This is accomplished by an inversion of the clock pulse sequence which is applied to the transfer registers. The charge in the pixels is then drained without contributing to the signal. Hence, N_{dark} can be calculated by the following equation:

$$N_{\mathrm{dark}} = \sqrt{N_{\mathrm{normal}}^2 - N_{\mathrm{backshift}}^2}. \quad (8)$$

The value of N_{dark} remains nearly constant in the typical operating temperature range of the pn-CCD on the satellite. Up to 190 K, a noise charge of typically three electrons is generated per pixel and image, i.e. within 80 ms (Fig. 11). The temperature-independent value is caused by the infrared light emission of the CAMEX. The noise contribution is hardly increased after a 10 MeV proton irradiation of 6.1×10^8 per cm^2.

Above 190 K (the exact temperature is device dependent), the noise increases steeply with the temperature and particle fluence because of the increase of the dark current.

3.2. Noise dependence of amplifying electronics on temperature

The dark current which is collected in the pixels does not contribute to the noise if the charge transfer direction is reversed. Only the on-chip electronics and the CAMEX preamplifier noise can change during a temperature scan since the other

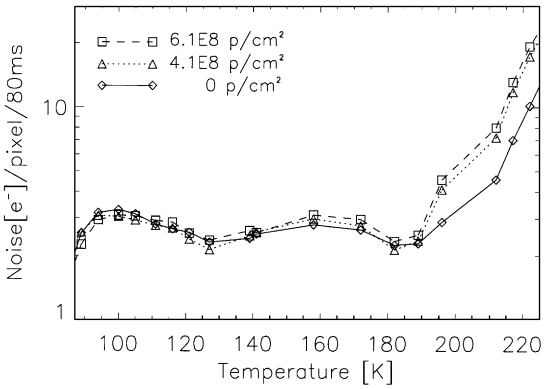

Fig. 11. Noise charge contribution of the bulk dark current per pixel and cycle time of 80 ms, as function of the temperature. The figure includes no other noise contributions, for example that of the readout electronics. The noise contribution remains nearly constant up to a temperature of 190 K since it is mainly determined by the infrared light emission of the CAMEX preamplifier. Above 190 K, the dark current noise increases steeply with the temperature due to the rise of the thermal generation current. For the same reason, the noise is then dependent on the proton fluence.

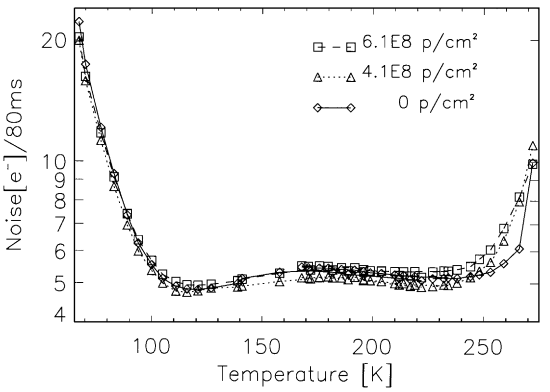

Fig. 12. Noise contribution of the amplifying electronics as a function of the operating temperature. The detector was operated with reverse charge transfer direction to eliminate the noise contribution of the pixels. Only the on-chip electronics and the CAMEX preamplifier are exposed to the temperature variation while the other electronics are kept at room temperature. Between 100 and 240 K, which includes the operating temperature range of the detectors on the satellites, the noise is at a minimum level of about five electrons. It is hardly dependent on the proton fluence. Above 240 K the noise increases with temperature and proton fluence.

electronics (e.g. the analog digital converter) is kept at a constant temperature.

Below 100 K, the noise increases steeply with decreasing temperature (Fig. 12). The noise is probably caused by a random telegraph signal (RTS) current generation in the FET due to traps. Between 100 and 240 K, the noise is about five electrons and nearly independent of the temperature. Above 240 K the noise increases with temperature and depends on the particle fluence. The rise in noise is probably mainly caused due to the thermal generation current which is collected at the anode. The noise of amplifying electronics is thus at its minimum in the possible operating temperature range of 140–190 K of the detectors on the satellites.

For a measurement of the CAMEX noise without the noise contribution of the on-chip electronics, the gate of the first FET of the on-chip electronics was grounded and the source connection removed. The remaining noise of the CAMEX and the readout electronics was found to be between 1.6 e^- and 2.6 e^- over the whole temperature range from 80 to 300 K (Fig. 13). No significant increase of noise could be observed after an α-particle fluence of 3.45×10^7 cm^{-2}. The main contribution to noise obviously results from the on-chip electronics, especially at the very low and high temperatures (compare Fig. 12).

3.3. *Transfer noise*

Trapping of single electrons by defects in the silicon lattice results in a noncomplete transfer of the signal charges. This underlies the Poisson statistics due to the discrete nature of the current transport. The transfer noise after n transfers N_{trans} can be modelled by the following basic approach with the reasonable assumption that the traps capture the electrons independently of each other:

$$N^2_{\text{trans},n} \sim S_0 - S_n = S_0(1 - \text{CTE}^n). \tag{9}$$

The term on the right describes the mean number of lost electrons after n pixel transfers of the signal ($0 \leqslant n \leqslant 199$). S_n is the number of signal electrons after n pixel transfers and S_0 is the number of signal electrons which are generated in the silicon by an

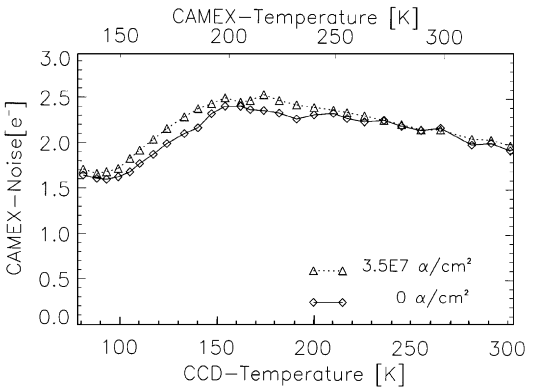

Fig. 13. Noise contribution of CAMEX preamplifier as function of the operating temperature. The measurement was performed without current through the first FET of the on-chip electronics to get no noise contribution of the CCD and its on-chip electronics. The temperature scale at the lower abscissa shows the CCD temperature while the upper scale shows the CAMEX temperature. The noise level between 1.5 e^- and 2.6 e^- over the complete temperature range is hardly dependent on the α-particle fluence of 3.5×10^7 cm^{-2} and relatively small compared to that of the total amplifying electronics (see Fig. 12). The noise increase below 100 and above 240 K, which is shown in Fig. 12, results obviously from the on-chip electronics. As a result, the CAMEX preamplifier shows no significant radiation damage after the α-particle irradiation.

X-ray photon with an energy of $E_{\text{X-ray}}$:

$$S_0[\text{e}^-] = E_{\text{X-ray}}[\text{eV}]/3.70\left[\frac{\text{e}^-}{\text{eV}}\right]. \tag{10}$$

According to the reason mentioned above, the CTI value is not constant but underlying some statistics. In addition, the occupation of traps fluctuates with the time because of the varying time difference between two transferred signal charge packets. Hence, the CTI is also varying. Moreover the CTI-correction for the "out of time" signals is wrong. "Out of time" photons hit the device during the transfer and not during the integration time of the CCD. Therefore the position allocation in transfer direction is wrong and the CTE correction too. Almost 6% of the X-rays are affected by this.

The transfer noise contributions before and after irradiation, can be separated in a first approach because the charge losses are caused by different trap types that are effective at rather different temperatures. The energy resolution after irradiation $\text{FWHM}^2_{\text{irrad}}$ and the amount of charge transfer efficiency caused by the particle exposure, CTE_{ir}, are then correlated by the following equation (for a uniform illumination with X-rays):

$$\begin{aligned}\text{FWHM}^2_{\text{irrad}} = \text{FWHM}^2_0 &+ a^2 2.355^2 \times 3.70^2 S_0 \\ &\times \frac{1}{199}\sum_{n=1}^{199}(1 - \text{CTE}^n_{\text{ir}}) \\ &+ 2.355^2 \times 3.70^2 N^2_{\text{dark}}\end{aligned} \tag{11}$$

FWHM_0 gives the energy resolution before irradiation. The second term describes the average transfer noise of all pixels of the transfer channel. Hence, the sum of the charge transfer losses are made up of the 199 pixels according to Eq. (9) with a proportionality factor '*a*' starting from pixel number 2 up to pixel number 200. CTE_{ir} is defined as $1 - \Delta\text{CTI}_{\text{ir}}$ with $\Delta\text{CTI}_{\text{ir}}$ as the increase of CTI due to an irradiation. The last term represents the noise contribution of the dark current increase after irradiation. The dark current noise contribution can be neglected for temperatures below 190 K (see Fig. 11). The proportionality factor '*a*' in Eq. (11) was evaluated for measurements at different temperatures, proton fluences and different X-ray energies as well as for measurements using the charge injection. As a result a value of 1.1 was obtained for '*a*'. The fluctuation of the results for this proportionality factor decreases with an increasing radiation exposure due to the prevailing of the transfer

Fig. 14. Mn-K_α and Mn-K_β spectra taken at different temperatures ranging from 67 up to 173 K. The spectrum without proton exposure is represented by the thin line whereas the spectrum after a 10 MeV proton fluence of 1.9×10^9 cm^{-2} is depicted by the thick line. At the lowest temperature of 67 K, the poor energy resolution is caused by the amplifying electronics. A high spectral resolution is obtained at a temperature of 114 K for the non-irradiated pn-CCD showing in this case a minimum charge transfer loss. The proton irradiation, however, causes high charge transfer losses due to the generated A-centres. This results in severe degradation of the spectrum at 114 K. The best energy resolution after irradiation was measured at the highest operating temperature of 173 K. At this temperature, most of the captured electrons are released by the A-centres early enough to be transferred with the other signal charges.

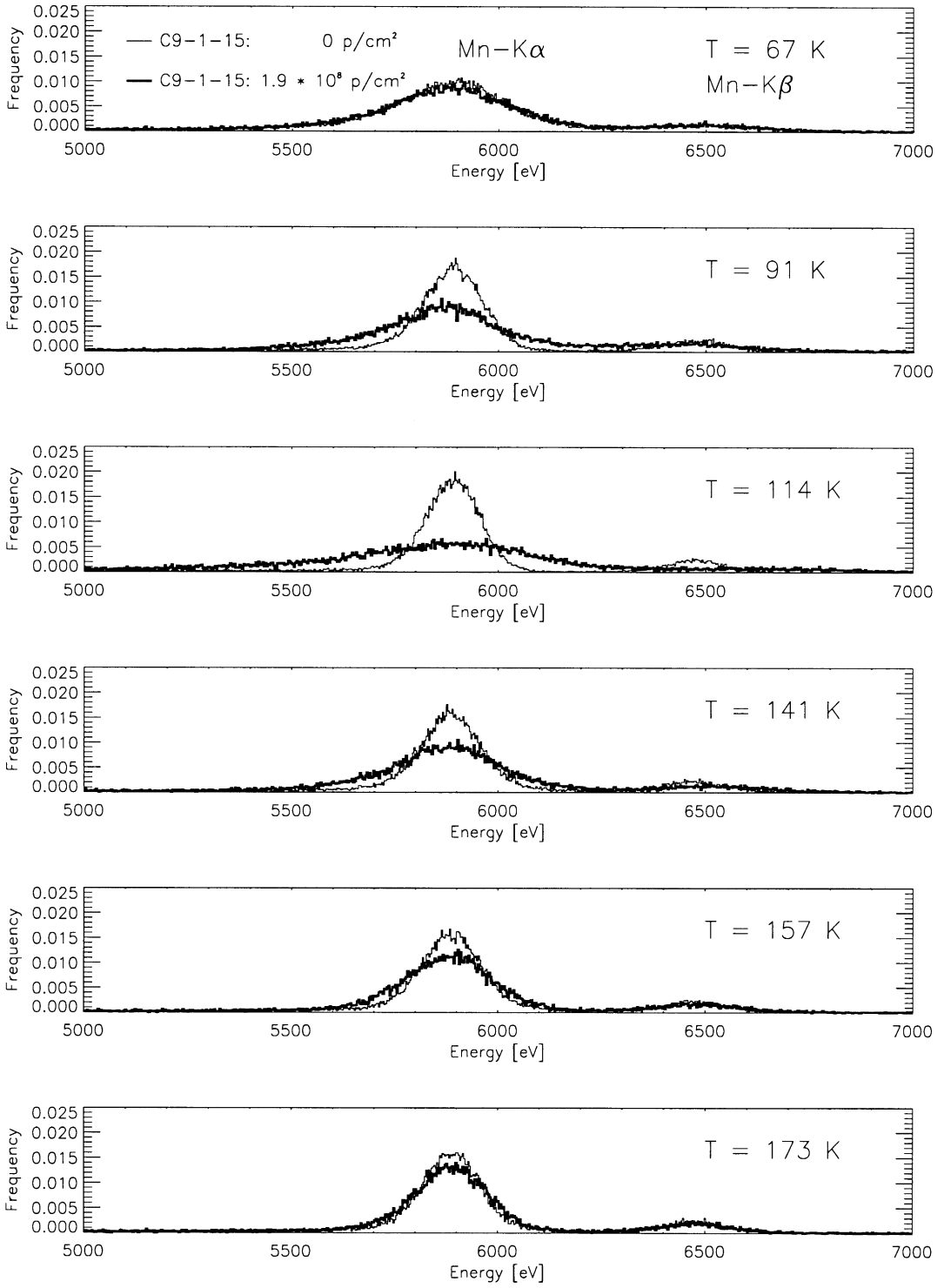
C9-1-15: 0 p/cm²
C9-1-15: 1.9 * 10⁸ p/cm²
Mn-Kα
Mn-Kβ
T = 67 K
T = 91 K
T = 114 K
T = 141 K
T = 157 K
T = 173 K
Frequency
Energy [eV]
0.025
0.020
0.015
0.010
0.005
0.000
5000
5500
6000
6500
7000

noise and a higher accuracy of the charge loss determination.

3.4. Energy resolution as function of temperature

For the evaluation of the energy resolution, simple corrections were applied as described in Ref. [7]. If we additionally take into account that not the best devices were chosen for the damaging radiation exposures, it is clear that the resulting FWHM values are slightly worse than they would be for the flight devices. Fig. 14 shows the spectra of the Mn-K_α (5894 eV) and Mn-K_β (6489 eV) lines with and without radiation damage for six different temperatures. For the lowest temperature of 67 K as well as for the highest of 173 K, the energy resolution is not significantly changed after a proton fluence of 1.9×10^9 p/cm^2. However, the energy resolution is bad at the low temperature in contrast to that of the high temperature. This is explained by the noise of the amplifying electronics which is, at 67 K, by a factor of four higher than for temperatures above 100 K (see Fig. 12). This noise contribution exceeds then even the Fano noise contribution. The spectrum taken at 114 K shows the worst degradation after proton exposure. The broadening of the lines is caused by the maximum charge transfer loss (see Fig. 6) which results in the maximum transfer noise. Before irradiation this temperature gave the best energy resolution due to the minimum charge transfer losses (see Fig. 5). Fig. 15 shows the evaluated FWHM of the Mn-K_α line as function of the operating temperature of the pn-CCD. A high spectral resolution before the irradiation and the best result after irradiation were obtained at the operating temperature of 173 K. The small improvement of energy resolution by the method of charge injection is also depicted in the figure.

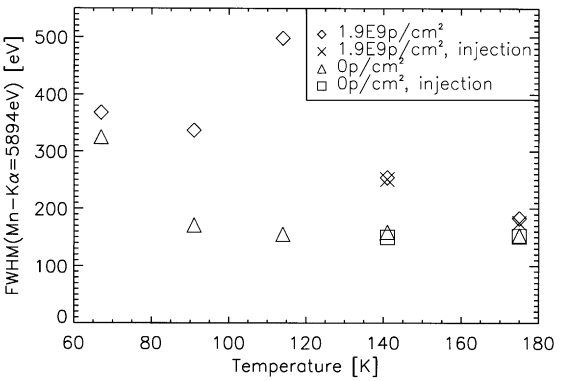

Fig. 15. The energy resolution of the Mn-K_α line is depicted as a function of the temperature after a 10 MeV proton exposure of 1.9×10^9 cm^{-2} and for comparison without radiation damage. The preferred operating temperature in a proton or α-particle environment is consequently a temperature of about 175 K where the FWHM had suffered the smallest degradation and is still close to the theoretical limit determined by the Fano noise. The small improvements due to charge injection are shown for the temperatures of 141 and 175 K.

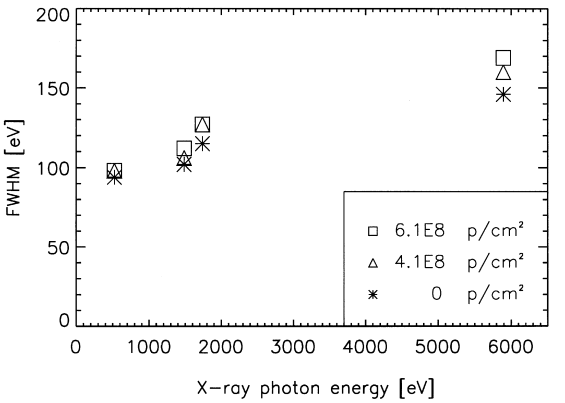

Fig. 16. The figure depicts the measured full-width at half-maximum of different X-ray energies. The asterisks show the energy resolution of devices without radiation damage. The triangles and the squares represent the degradation after 10 MeV proton fluences of 4.1×10^8 and 6.1×10^8 cm^{-2}, respectively. At the used operating temperature of 175 K, a high energy resolution over the complete energy range is maintained.

3.5. Spectra of different X-ray energies

Since the charge transfer losses depend on the number of transferred electrons, and the Fano noise increases with the X-ray energy, the resulting energy resolution depends on the X-ray energy. The energy resolution of four different X-ray energies (530 up to 5894 eV) is shown in Fig. 16 for different proton exposures at an operating temperature of 175 K. The measured degradation by a 10 MeV proton fluence of 6.1×10^9 cm^{-2} is less than 20% for all energies. In this sense, Fig. 16 displays the

maximum change in energy resolution for the 10 yr XMM mission.

3.6. Energy resolution after α-particle irradiation

The energy resolution of the Mn-K_α was not degraded after a 5.5 MeV α-particle exposure of $5.0 \times 10^5\,cm^{-2}$. However after a fluence of $4.2 \times 10^7\,cm^{-2}$ and without changing the MIS-voltage, the FWHM was degraded to about 260 eV. Both measurements were carried out at a temperature of 143 K. As in the case of the proton irradiation, we expect a dramatic improvement in the energy resolution at higher temperatures.

3.7. X-ray irradiation

The energy resolution of the detector remained unchanged after irradiation with soft X-rays of an Fe^{55}-source at a dose level of 23 krad. We measured a FWHM of 145 eV for the Mn-K_α-line at 5894 eV, and a FWHM of 97 eV for the Si-K_α-line at 1739 eV, both at an operating temperature of 143 K. In particular, a voltage adjustment to compensate the charging of the oxide and nitride in the passive MIS-gates was not necessary. The performance of the detector system including the CAMEX preamplifier and digital TIMEX chip was not affected by this dose of ionizing radiation. This behaviour was indeed expected since ionizing damage usually occurs at higher dose levels and the X-ray energy is too low for displacement damage.

4. Summary and conclusions

Particle irradiation of the pn-CCD causes radiation damage due to the generation of defects in the silicon lattice. These defects can act as traps and cause a charge transfer loss of the signal electron packet. Furthermore, the defects can take effect as generation centres for electron–hole pairs and contribute to the dark current collected in the pixels. In the operating temperature range of 140–190 K for the pn-CCD on the X-ray satellite missions, the charge transfer is limited by three trap types. The titanium impurity is already present before irradiation and degrades the CTE maximal at a temperature of about 180 K. The A-centre, an oxygen-vacancy defect, deteriorates the CTE most strongly at 115 K. The charge transfer losses due to the A-centre decrease with increasing temperature. However, the whole relevant temperature range is affected by this trap type. Another trap type with minor effect on the charge transfer could be observed after irradiation with 5.5 MeV α-particles. The trap type corresponds with the divacancy defect according to several evidences, e.g. the dependence of its occurrence on the nonionizing energy loss per particle.

The charge transfer loss in the pn-CCD is nearly completely caused by trapping of signal electrons. After irradiation, the CTE is at high temperatures (175 K) higher than at low (140 K) operating temperatures because of the A-centre. Before irradiation, the performance with regard to the temperature was vice versa due to titanium as dominant trap type. The best charge transfer performance was measured after a change from 0 to −15 V of the voltage applied to the MIS gate which is located between the transfer registers. The method of charge injection improves the CTE significantly at an operating temperature of about 120 K before irradiation. After particle exposure however, the charge injection results only in minor changes of the already degraded CTE.

The square of the transfer noise is correlated by a proportionality factor of 1.2 with the charge transfer loss. While the energy resolution is deteriorated at low temperatures by the A-centre, it is degraded at high temperatures above 190 K due to an increased thermal generation current in the pixels. The noise of on-chip JFET amplifiers is only affected at still higher temperatures. After 10 MeV-proton or 5.5 MeV-α-particle fluences in the order of 10^9 and $10^7\,cm^{-2}$, respectively, a good detector performance is maintained at an operating temperature of about 175 K. Hence, we operate the pn-CCD relative independently of all kinds of radiation damage. Of course, a charge loss correction has to be performed in order to obtain a good energy resolution.

The ionizing radiation of soft X-rays did not affect the detector performance up to the highest tested dose level of 23 krad. The CAMEX preamplifier chip and the digital TIMEX chip

showed no degradation after particle and X-ray exposures.

The charge transfer loss of the flight-type pn-CCDs was reduced by narrowing the transfer channel width in comparison to the prototype devices. However a higher generation probability of the A-centres was found in the flight-type CCDs and hence higher charge transfer losses after proton irradiation. This was caused by a higher oxygen concentration of the new silicon wafers.

The oxygen concentration of FZ silicon is usually below the detection limit of standard diagnostic methods. The dependence of the charge transfer loss on the oxygen concentration could be used for a relative determination of the oxygen concentration in silicon as shown for the prototype and flight type silicon. An absolute measurement would be possible using wafers with a high but calibrated oxygen concentration as reference samples.

Acknowledgements

We wish to thank W. Assmann and W. Dünnweber for their support at the TANDEM accelerator in Garching as well as P. Solc for the mounting and bonding of the devices. The project was supported by the Deutsche Agentur für Raumfahrtangelegenheiten (DARA) under contract No. 50 0X 93025/-XMM-EPIC and by the EUROPEAN SPACE AGENCY under contract No. 8873/90/NL/PB(SC) CCN No. 2.

References

[1] H. Soltau et al., Nucl. Instr. and Meth. A 439 (2000) 547.
[2] R. Hartmann, K.-H. Stephan, L. Strüder, Nucl. Instr. and Meth. A 439 (2000) 216.
[3] D. Lumb et al., Proc. SPIE 2808 (1996) 326.
[4] G. Richter, G. Hasinger, P. Friedrich, K. Fritze, J. Trümper, H. Bräuninger, P. Predehl, R. Staubert, E. Kendziorra, Exp. Astronom. 159 (1995) 162.
[5] N. Meidinger, H. Soltau, L. Strüder, C. v. Zanthier, IEEE Trans. Nucl. Sci. NS-42 (6) (1995) 2066.
[6] N. Meidinger et al., Nucl. Instr. and Meth. A 377 (1996) 299.
[7] N. Meidinger, B. Schmalhofer, L. Strüder, IEEE Trans. Nucl. Sci. 45 (6) (1998) 2849.
[8] E. Pinotti, Studio teorico e sperimentale di fenomeni di generazione in silicio ai fini del miglioramento delle prestazioni di CCD per astronomia X, Ph.D. Thesis, Politecnico di Milano, 1995.
[9] N. Krause et al., Nucl. Instr. and Meth. A 439 (2000) 228.